RSC Advances

PAPER

View Article Online
View Journal | View Issue

Cite this: *RSC Adv.*, 2021, **11**, 33662

Ratiometric fluorescence probe of Cu^{2+} and biothiols by using carbon dots and copper nanoclusters†

Ning Zhao,[a] Jianqiang Song,[a] Zheng Huang,[a] Xiuying Yang,[b] Yousheng Wang[b] and Longshan Zhao *[a]

A novel dual-emission ratiometric fluorescent probe based on N-doped yellow fluorescent carbon dots (y-CDs) and blue fluorescent copper nanoclusters (CuNCs) was established for quantitative determination of Cu^{2+} and biothiols. In this work, the Cu^{2+}-(y-CDs) complexes formed by the chelation of y-CDs with Cu^{2+}, showed an absorption peak at 430 nm that not only enhanced the fluorescence of y-CDs through inhibiting photoinduced electron transfer (PET) but also effectively quenched the fluorescence of CuNCs due to Förster resonance energy transfer (FRET). In addition, the chelation of y-CDs with Cu^{2+} could be inhibited by biothiols that prevented the fluorescence of y-CDs from being enhanced and the fluorescence of CuNCs from being quenched. On account of the changes of ratiometric signal, a dual-emission fluorescence probe for Cu^{2+} and biothiols determination was achieved. The proposed method exhibited high sensitivity for Cu^{2+} and biothiols in the ranges of 0.5–100 μM and 0.8–50 μM and the limits of detection (LODs) of Cu^{2+}, glutathione (GSH), cysteine (Cys) and homocysteine (Hcy) were 0.21 μM, 0.33 μM, 0.39 μM and 0.46 μM, respectively. Subsequently, the established strategy presented an application prospect for the detection of Cu^{2+} and biothiols in real samples.

Received 2nd August 2021
Accepted 8th October 2021

DOI: 10.1039/d1ra05854a

rsc.li/rsc-advances

1. Introduction

The copper ion (Cu^{2+}), as an essential nutrient for humans, animals and plants, can regulate various physiological functions of humans.[1] However, deficiency or excess of Cu^{2+} may lead to many diseases, such as Wilson disease, Menkes disease, cardiovascular disease and cancer.[2] Besides, due to its wide applications in industry and agriculture, the excessive accumulation of Cu^{2+} may also cause serious environmental pollution and imbalance of ecosystems.[3] On the other hand, biothiols, as an important part of many proteins and small molecules in organisms, mainly include cysteine (Cys), homocysteine (Hcy) and glutathione (GSH), and play irreplaceable roles in maintaining intracellular redox activity and regulating cellular function.[4,5] Studies have found that the abnormal levels of biothiols in the body are associated with some diseases, such as skin lesions, liver damage, Alzheimer's disease, cardiovascular disease and cancer.[6] Hence, developing a sensitive and effective strategy for Cu^{2+} and biothiols detection is meaningful. To date, various analytical methods have been developed for Cu^{2+} determination containing atomic absorption spectrometry,[7] inductively coupled plasma mass spectrometry,[8] electrochemistry[9] and colorimetry,[10] and for the detection of biothiols, methods such as electrochemiluminescence,[11] electrochemistry,[12] colorimetry[13] and high performance liquid chromatography[14] have been demonstrated. Most of these methods, however, were restricted by expensive instrument, complicated operation, time-consuming and the use of organic reagent. Hence, it is urgent to establish simple, fast and effective methods for Cu^{2+} and biothiols detection.

In recent years, carbon dots (CDs), a class of "zero-dimensional" nanomaterials, have attracted extensive attentions. The differences from semiconductor quantum dots (QDs) and other fluorescent materials are that CDs have great optical properties, low toxicity, good aqueous solubility and stability.[15,16] In view of these unique properties, CDs have shown great potentials in sensing, bioimaging, drug delivery, photodynamic therapy and medical diagnosis.[17,18] At present, to improve the properties of CDs, different synthesis methods using various precursors as raw materials have been gradually developed, which are primarily divided into the top-down method with complex synthesis conditions and the bottom-up method with high productivity.[19] Furthermore, studies have found that heteroatom doping can improve the fluorescence properties of CDs and enlarge their application scopes.[20] Consequently, the prepared CDs are usually composed of sp^2/sp^3 carbon, oxygen/nitrogen-based groups and post-modified chemical groups in recent years.[21]

[a]*School of Pharmacy, Shenyang Pharmaceutical University, 103 Wenhua Road Shenhe District, Shenyang, Liaoning, 110016, P. R. China. E-mail: longshanzhao@163.com; Fax: +86-24-4352-0571; Tel: +86-24-4352-0571*

[b]*Hainan Vocational University of Science and Technology, Key Laboratory of Medicinal and Edible Plants Resources of Hainan Province, Haikou, Hainan 571126, China*

† Electronic supplementary information (ESI) available. See DOI: 10.1039/d1ra05854a

Metal nanoclusters (NCs), a class of nanomaterials with core–shell structures, are made up of numerous metal atoms and ligands, and have aroused a considerable research interest. Owing to the discontinuous band structures and molecule-like properties, metal NCs show emission characteristics from visible to near-infrared light, and unique physicochemical properties including large Stokes shift, excellent optical stability and good biocompatibility.[22] Therefore, various novel metal NCs, especially AuNCs and AgNCs, have developed rapidly over the past few decades, and possess widespread applications in bioimaging, sensor and other fields.[23] However, CuNCs, which have similar fluorescence characteristics to AuNCs and AgNCs, have attracted increasing interest due to the low price of raw materials. Moreover, the stability and solubility of CuNCs have been improved significantly by modifying its surface with ligands,[24] making CuNCs one of the suitable candidates for bioimaging, sensor and catalysis applications.

To our knowledge, most of the previously reported fluorescence approaches for the simultaneous determination of Cu^{2+} and biothiols were usually performed by recording the changes of single fluorescence signal.[25,26] Nevertheless, the main limitation of this type of fluorescence probe with single emission intensity is that the detection is easily affected by environmental condition, background fluorescence, instrumental efficiency and probe concentration.[27,28] In contrast, ratiometric fluorescence assays utilizing the intensity ratio of two fluorescence peaks as analytical signal, can alleviate these problems by providing an intrinsic self-calibration function, and then achieve more sensitive and accurate determination for analytes.[29] To date, various ratiometric fluorescence probes have been constructed *via* forming a core–shell structure or covalent binding. For instance, Zeng *et al.*[30] designed a core–shell structure made up of YVO_4:Eu^{3+} nanoparticles and CDs to construct a sensing system for Cu^{2+} and biothiols detection. Ying *et al.*[31] constructed an ion imprinted fluorescent probe based on amino-riched CDs and carboxyl-riched CdTe QDs for detecting Fe^{3+} and Cu^{2+} at the same time. However, the complicated synthesis, high cytotoxicity, low biocompatibility, time-consuming and cumbersome construction processes of core–shell structure and covalent bond severely limited the further applications of these ratiometric fluorescence probes. Accordingly, developing a simple, efficient, environmentally friendly and self-assembly ratiometric fluorescent method for Cu^{2+} and biothiols determination is of high demand.

Herein, a dual-emission ratiometric fluorescent probe based on CDs and CuNCs was constructed and firstly applied to detect Cu^{2+} and biothiols (Scheme 1). The N-doped yellow CDs (y-CDs), synthesized utilizing *o*-phenylenediamine (OPD) and urea as precursors by one-pot hydrothermal method, and glutathione modified blue CuNCs, synthesized by one-pot synthesis method, exhibited strong fluorescence at 567 and 450 nm, respectively. In the strategy, the chelation of y-CDs with Cu^{2+} formed the Cu^{2+}-(y-CDs) complexes with a new absorption peak appearing in ultraviolet region. The formation of Cu^{2+}-(y-CDs) complexes led to the fluorescence enhancement of y-CDs by inhibiting photoinduced electron transfer (PET), accompanied with the fluorescence quenching of CuNCs on account of Förster resonance energy transfer (FRET) between CuNCs and Cu^{2+}-(y-CDs) complexes. Upon the addition of biothiols, the strong chelation between biothiols and Cu^{2+} removed Cu^{2+} from the y-CDs surface, resulting in the fluorescence quenching of y-CDs and the fluorescence recovery of CuNCs. Hence, in this

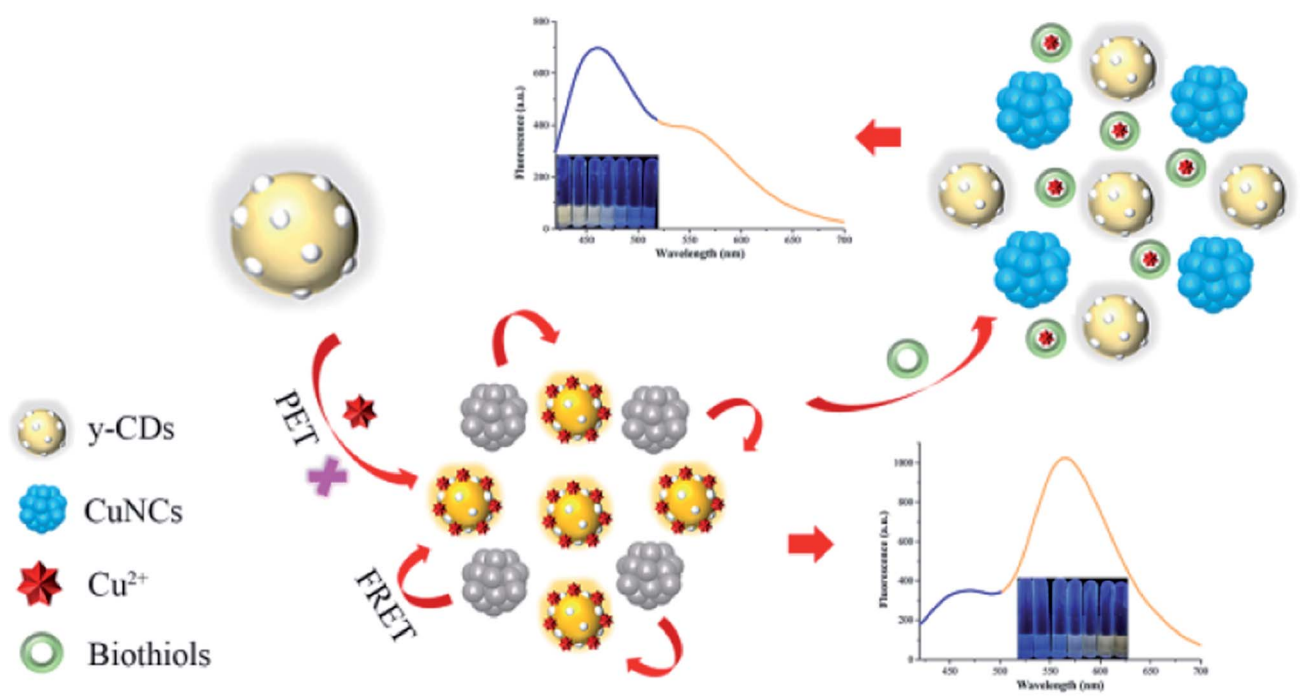

Scheme 1 Schematic illustration of the ratiometric fluorescence probe for Cu^{2+} and biothiols based on y-CDs and CuNCs.

study, the synthesized y-CDs and CuNCs had the advantages of simple synthesis process, low toxicity and excellent water solubility. And the ratiometric fluorescent detection method constructed by self-assembly was not susceptible to environmental condition, background fluorescence, instrumental efficiency and probe concentration. Therefore, this study used y-CDs and CuNCs to construct a dual-mechanism-based ratiometric fluorescent probe for the first time to simultaneously detect Cu^{2+} and biothiols in real samples, which provided great application prospects.

2. Experimental section

2.1. Materials and chemicals

O-phenylenediamine (OPD, 99.5%) and urea were provided by Rhawn Chemical Technology Co., Ltd. (Shanghai, China) and Kemiou Chemical Reagent Co., Ltd. (Tianjin, China), respectively. $CuSO_4 \cdot 5H_2O$, $Cu(NO_3)_2 \cdot 3H_2O$, $AgNO_3$, $Al(NO_3)_3$, $BaCl_2$, $CdCl_2$, $Fe_2(SO_4)_3$ and $LiBr \cdot H_2O$ were obtained from Damao Chemical Reagent Factory (Tianjin, China). Ascorbic acid (AA, >99.0%), cysteine (Cys, 98%), $HgSO_4$, $MnCl_2$, $NiSO_4$, $PbCl_2$, alanine (Ala) and glycine (Gly) were acquired from Macklin Biochemical Co., Ltd. (Shanghai, China). Glutathione (GSH, 97%), homocysteine (Hcy, 95%), asparagine (Asn), aspartic acid (Asp), lysine (Lys), methionine (Met), proline (Pro), serine (Ser) and threonine (Thr) were bought from Bide Pharmatech Ltd. (Shanghai, China). Arginine (Arg) was supplied by Xiya Chemical Technology Co., Ltd. (Shandong, China). $CaSO_4 \cdot 2H_2O$, KCl, $Mg(NO_3)_2 \cdot 6H_2O$, NaCl and $ZnCl_2$ were provided by Hengxing Chemical Reagent Co., Ltd. (Tianjin, China). Other amino acids including histidine (His), phenylalanine (Phe), glutamine (Gln), glutamic acid (Glu), isoleucine (Ile), leucine (Leu), tryptophan (Trp), tyrosine (Tyr) and valine (Val) were purchased from Yuanye Biotechnology Co., Ltd. (Shanghai, China). Distilled water from Wahaha Co., Ltd. (Hangzhou, China) was used to prepare solutions throughout the experiment. All the reagents used in this study were analytical grade and used directly as received without further purification.

2.2. Instruments

The transmission electron microscopy (TEM) and high-resolution TEM (HRTEM) images acquired with a JEM-2100F transmission electron microscope (JEOL, Japan) were used to analyze the morphologies of y-CDs and CuNCs. The X-ray photoelectron spectroscopy (XPS) was obtained from an Escalab250Xi (Thermo Fisher, USA). Fourier transform infrared spectroscopy (FT-IR) was recorded by a Nicolet IS50 FT-IR spectrometer (Thermo Fisher, USA). The zeta potentials of the y-CDs and CuNCs were analyzed by a Malvern Zetasizer Nano-ZS90 (Malvern, USA). The fluorescence quantum yield and lifetime were measured by Hamamatsu C9920-02G (Hamamatsu, Japan) and FLS 1000 fluorescence spectrometer (Edinburgh, UK), respectively. The fluorescence spectrum was recorded with a F97 (Shanghai Lengguang Technology Co., Ltd. China). Ultraviolet-visible (UV-vis) absorption spectrum was measured using an UV-5500PC spectrophotometer (Shanghai Metash Instruments Co., Ltd. China).

2.3. Synthesis of y-CDs

The y-CDs were synthesized *via* hydrothermal method. Briefly, 0.1 g OPD and 0.2 g urea were mixed and fully dissolved in 12 mL water *via* ultrasound. Then, the solution was transferred into a Teflon-lined autoclave and heated at 160 °C for 5 h. The obtained yellow solution was centrifuged for 20 min at 12 000 rpm and filtered with a 0.22 μm filter membrane to remove large particles. After that, the supernatant was purified by dialysis bag (500 Da) with distilled water for 12 h. Finally, the purified y-CDs powder obtained by freeze-drying was stored at 4 °C for further experiment.

2.4. Synthesis of CuNCs

The CuNCs were prepared using a published report with minor modification.[32] Firstly, 0.5 mL $CuSO_4$ (50 mM) and 2 mL GSH (50 mM) were mixed and continually stirred until the solution turned to pale yellow. After that, with the addition of NaOH (1 M), the suspension changed to transparency. Then, the pH of the solution was adjusted to 8 by using NaOH solution after adding 2.5 mL of AA (11 mg mL^{-1}). The mixed solution was incubated at 85 °C for 7 h in an oil bath. Finally, the resulting solution was dialyzed with dialysis bag (500 Da) for 12 h to remove the residuum. The freeze-dried CuNCs powder was redissolved in 5 mL of water and stored at 4 °C for further use.

2.5. Detection of Cu^{2+} and biothiols

For the detection of Cu^{2+}, 20 μL of the y-CDs (15 mg mL^{-1}) and 200 μL of Cu^{2+} solution with different concentrations were added to 2.6 mL of PBS buffer solution (pH 8, 0.1 M), and the mixed solution was incubated at 60 °C for 50 min. After that, 180 μL of the CuNCs solution (10 mg mL^{-1}) was added and the solution was vortexed strongly for 3 min at room temperature before recording the intensity ratio with the excitation wavelength at 400 nm. The selectivity of the Cu^{2+} detection was evaluated by replacing Cu^{2+} with other metal ions under the same experimental conditions as mentioned above.

For the biothiols determination, GSH, Cys and Hcy in different amounts and concentrations were mixed with 200 μL of Cu^{2+} (70 μM) solution, respectively, and the solutions were vortexed for 8 min at room temperature. After adding 20 μL of the y-CDs (15 mg mL^{-1}), the mixed solutions were diluted to 2.8 mL with PBS buffer solution (pH 8, 0.1 M) and then incubated at 60 °C for 50 min. Subsequently, 180 μL of the CuNCs solution (10 mg mL^{-1}) was added and the solutions were vortexed intensely for 3 min at room temperature, following the intensity ratios were measured at 400 nm excitation. To investigate the selectivity of the biothiols detection, other amino acids were added instead of biothiols in the same way as described above.

2.6. Detection of Cu^{2+} and biothiols in real samples

The practicability of the prepared ratiometric fluorescence probe was estimated by detecting Cu^{2+} in tap water, river water, grape juice and peach juice samples, and biothiols in human serum samples. The tap water and river water samples were

obtained from our laboratory and Shahe River (Benxi, China), separately. The water samples were first centrifuged at 4200 rpm for 10 min, and then filtered with 0.22 μm filter membranes. The grape juice and peach juice samples purchased from a local market were filtered, and 20-fold diluted with distilled water. Human serum samples were collected from healthy volunteers.

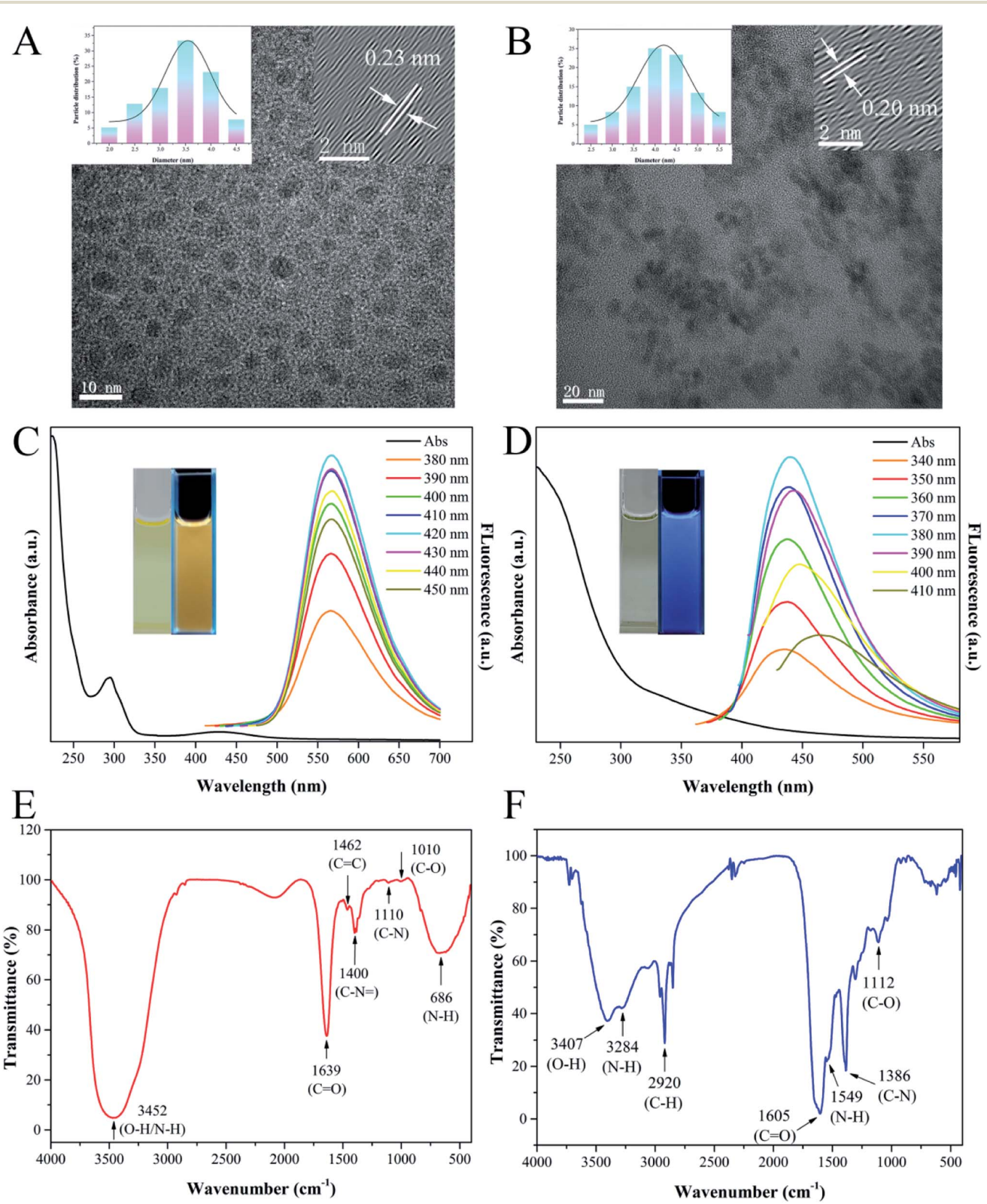

Fig. 1 TEM images of the (A) y-CDs and (B) CuNCs. Insets show the corresponding particle size distribution and HRTEM images. UV-vis absorption spectra and fluorescence spectra for the (C) y-CDs and (D) CuNCs at various excitation wavelengths. Insets: images of the y-CDs and CuNCs under natural light and 365 nm UV light lamp. FT-IR spectra of (E) y-CDs and (F) CuNCs.

After centrifugation and filtration, the supernatant was 100-fold diluted with PBS buffer solution. Finally, all pretreated water and beverage samples were spiked with various concentrations of Cu^{2+} solution, and the serum samples were spiked with different concentrations of GSH, respectively.

3. Results and discussion

3.1. Characterizations of y-CDs and CuNCs

Firstly, the morphology and size of as-synthesized y-CDs and CuNCs were characterized by TEM. As shown in Fig. 1A, the TEM image exhibited that the y-CDs were well-dispersed ranging from 2.04 to 4.46 nm with a mean diameter of approximately 3.42 nm (inset in Fig. 1A). This was similar to the result of the hydrodynamic size distribution in Fig. S1.† In the HRTEM image (inset in Fig. 1A), a clear lattice spacing of y-CDs was 0.23 nm, corresponding to the (100) facet of graphite.[33] Fig. 1B illustrated that CuNCs possessed a good dispersity with an average size of 4.17 nm and a lattice spacing of 0.20 nm (inset in Fig. 1B).

The optical properties of y-CDs and CuNCs were investigated by the analysis of UV-vis absorption and fluorescence spectra. As presented in Fig. 1C, there were two obvious UV-vis absorption bands at 282 and 430 nm in the spectrum of y-CDs, which were ascribed to the π–π* transition of C=C and the n–π* transition of C=O, respectively. And the y-CDs exhibited excitation-independent property with different excitations varying from 380 to 450 nm, and showed yellow luminescence under the 365 nm UV light (inset in Fig. 1C). Besides, it could be seen from Fig. 1D that CuNCs possessed a strong absorption in UV region, and displayed blue luminescence with excitation-dependent feature.

Subsequently, the structures and surface functional groups of y-CDs and CuNCs were described by FT-IR spectroscopy. As plotted in Fig. 1E, the broad absorption peak at 3452 cm^{-1} was ascribed to the O–H/N–H stretching vibrations, showing the existence of amino and oxygen functional groups on the surface of y-CDs. The appearance of absorption peak around 1639 cm^{-1} was assigned to the C=O stretching vibration. The existence of absorption bands at 1462 and 1400 cm^{-1} corresponded to the stretching vibrations of C=C and C–N=.[34] Furthermore, the peaks located at 1110 and 1010 cm^{-1} were attributed to C–N and C–O stretching vibrations.[35] The broad absorption band at 686 cm^{-1} was attributed to N–H.[36] The above results demonstrated that the N as a dopant was successfully doped in y-CDs. The FT-IR spectroscopy of CuNCs (Fig. 1F) showed that the absorption bands at 3407 and 2920 cm^{-1} were related to O–H and C–H stretching vibrations, respectively. The stretching vibration and bending vibration caused by the N–H bond appeared at 3284 and 1549 cm^{-1}. There existed a strong absorption peak at 1605 cm^{-1}, demonstrating the presence of C=O stretching vibration. Besides, the peaks around 1386 and 1112 cm^{-1} were associated with C–N and C–O, respectively.[37] This analysis revealed the presence of –COOH and $–NH_2$ groups on the CuNCs surface.

The element components and functional groups of y-CDs and CuNCs were further confirmed by XPS spectroscopy, and the results were depicted below. It could be seen from Fig. 2A that the full scan XPS spectrum of y-CDs had three distinct peaks at 284, 399 and 531 eV, representing C 1s, N 1s and O 1s, separately. The high-resolution C 1s spectrum (Fig. 2B) with three different peaks at 284.1, 285.4, and 288.1 eV indicated that carbon mainly existed in the forms of C–C/C=C, C–N/C–O, and C=O, respectively.[38] As plotted in Fig. 2C, the N 1s spectrum exhibited three peaks at 398.8, 399.5 and 400.1 eV, which were respectively assigned to N–H, $N–(C)_3$ and N–C–N.[34] For the high-resolution spectrum of O 1s (Fig. 2D), there were two peaks at 531.0 and 532.2 eV, which were consistent with C=O and C–OH/C–O–C, respectively.[39] These XPS results were in good accordance with the FT-IR results, confirming the presence of –OH, $–NH_2$ and –CO– functional groups on y-CDs surface. The full scan XPS spectrum (Fig. 2E) described that CuNCs were composed of S, C, N, O and Cu. As plotted in Fig. 2F, the high-resolution Cu 2p spectrum presented two characteristic peaks at 931.9 and 951.8 eV, which were assigned to the Cu $2p_{3/2}$ and Cu $2p_{1/2}$.[40] These XPS results of CuNCs were consistent with the results of FT-IR analysis.

3.2. Stability of y-CDs

The stability, one of the important properties of nanometer materials, was researched in this experiment to facilitate the analysis and detection of y-CDs. Therefore, the radiation time, ionic strength and storage time that affected the fluorescence intensity of y-CDs were studied. It could be seen from Fig. S2A† that the fluorescence intensity of y-CDs decreased slowly, while it could retain about 88% under continuous radiation by UV light at 365 nm for 100 min, demonstrating that the y-CDs had great photobleaching resistance. As presented in Fig. S2B,† the fluorescence intensity of the y-CDs was hardly affected by high concentration NaCl solution, which showed that the y-CDs were highly stable in salt medium. As depicted in Fig. S2C,† with the extension of storage time, the fluorescence intensity of y-CDs changed slightly, so the y-CDs were extremely stable for 60 days. In short, the results mentioned above indicated that the prepared y-CDs had great stability and were suitable for applications in real samples. And the y-CDs showed the quantum yield up to 6.44%.

3.3. Detection mechanism of Cu^{2+} and biothiols

In this work, we evaluated the feasibility of detecting Cu^{2+} and biothiols by the analysis of UV-vis absorption and fluorescence spectra. As displayed in Fig. 3A, Cu^{2+} could enhance the fluorescence of y-CDs at 567 nm significantly, while the fluorescence of CuNCs at 450 nm showed a negligible change. This might be due to the coordination of Cu^{2+} with more nitrogen-containing groups on the surface of y-CDs.[41] It could be clearly seen from Fig. 3B that the Cu^{2+}-(y-CDs) complexes formed by the coordination of Cu^{2+} with y-CDs presented an apparent absorption peak at 430 nm. However, the fluorescence of CuNCs decreased significantly when it was added to the Cu^{2+}-(y-CDs) complexes solution. Therefore, the quantitative determination of Cu^{2+} was achieved based on the fluorescence changes of y-CDs and CuNCs. With the introduction of biothiols, the enhanced fluorescence of y-CDs by Cu^{2+} could be quenched while the fluorescence of CuNCs could be restored (Fig. 3C, such as GSH). This might be due to the

fact that the addition of biothiols inhibited the formation of Cu^{2+}-(y-CDs) complexes, resulting in a significant decrease in absorption at 430 nm (Fig. 3B). Hence, a convenient and efficient ratiometric fluorescent probe was established and applied to the detection of biothiols.

The enhanced fluorescence of y-CDs was possibly connected with the chelation of Cu^{2+} with y-CDs that inhibited PET process. To verify the mechanism, a series of measurements were performed by FT-IR, Raman scattering and TEM techniques. Fig. 3B showed that in the presence of Cu^{2+}, a new UV-

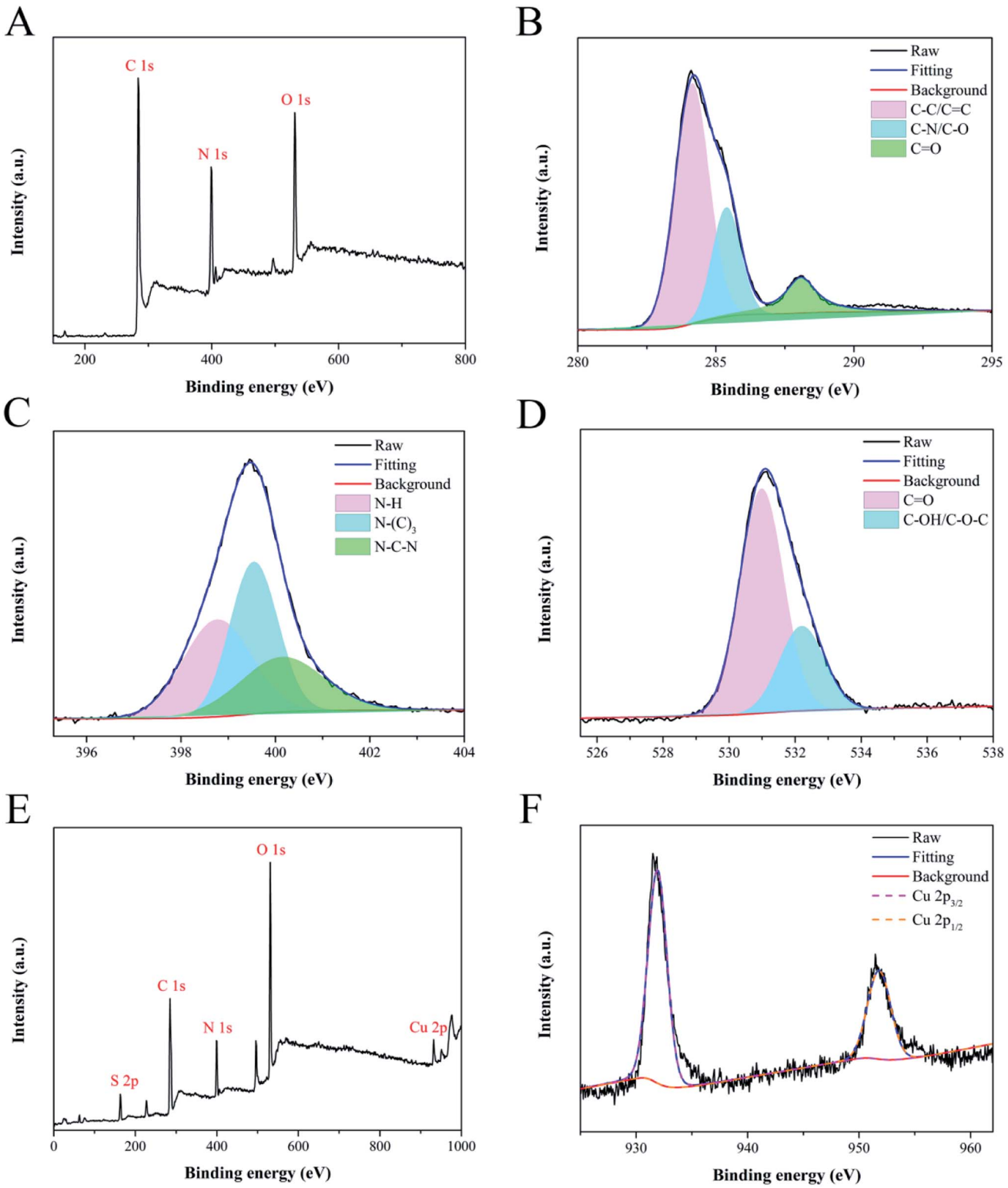

Fig. 2 The full XPS spectrum of y-CDs (A) and high-resolution XPS spectra of C 1s (B), N 1s (C) and O 1s (D). XPS survey spectrum of CuNCs (E) and high-resolution XPS spectrum of Cu 2p (F).

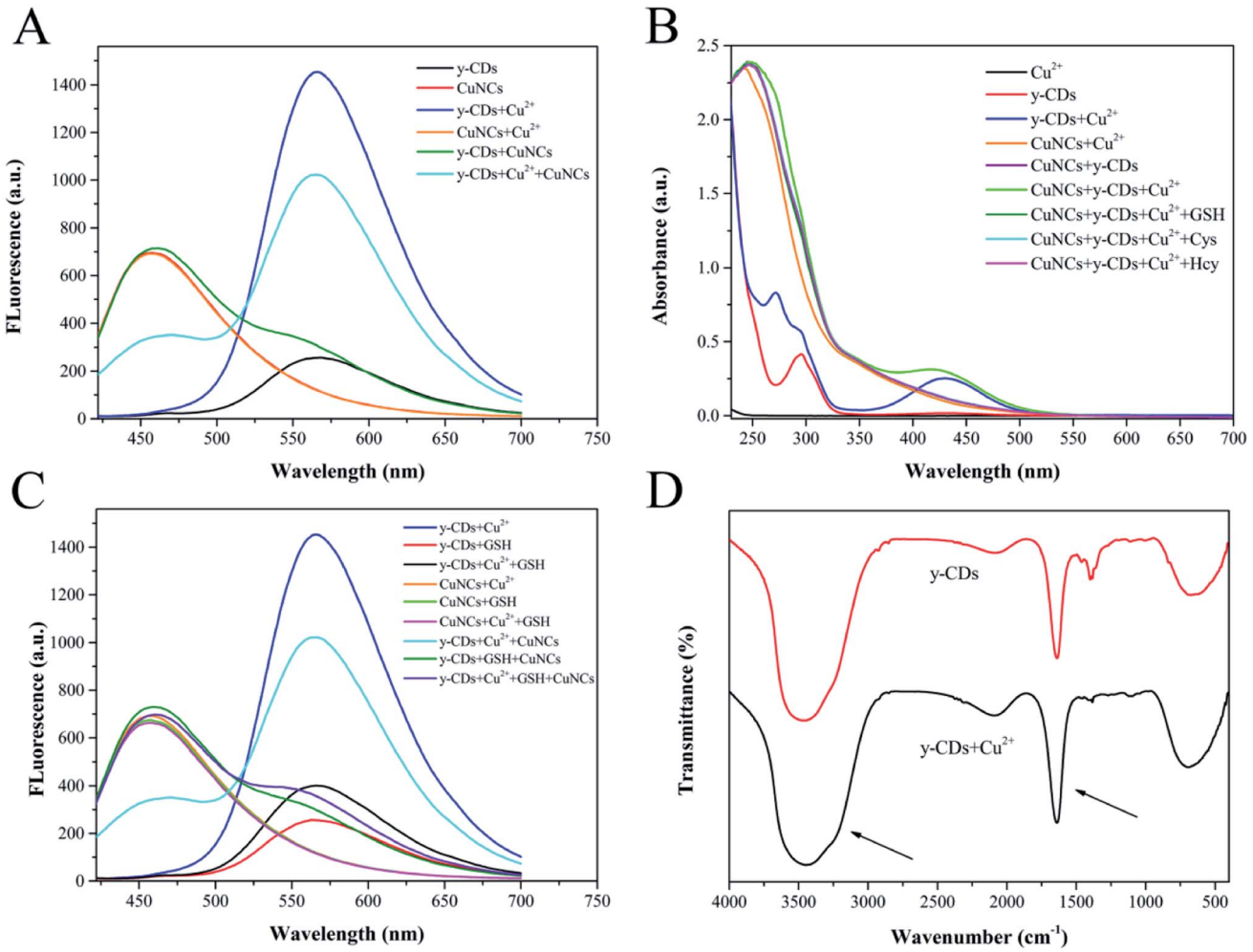

Fig. 3 (A) Fluorescence emission spectra of y-CDs, CuNCs, y-CDs + Cu^{2+}, CuNCs + Cu^{2+}, y-CDs + CuNCs, y-CDs + Cu^{2+} + CuNCs. (B) UV-vis absorption spectra of Cu^{2+}, y-CDs, y-CDs + Cu^{2+}, CuNCs + Cu^{2+}, CuNCs + y-CDs, CuNCs + y-CDs + Cu^{2+}, CuNCs + y-CDs + Cu^{2+} + GSH, CuNCs + y-CDs + Cu^{2+} + Cys, CuNCs + y-CDs + Cu^{2+} + Hcy. (C) Fluorescence emission spectra of y-CDs + Cu^{2+}, y-CDs + GSH, y-CDs + Cu^{2+} + GSH, CuNCs + Cu^{2+}, CuNCs + GSH, CuNCs + Cu^{2+} + GSH, y-CDs + Cu^{2+} + CuNCs, y-CDs + GSH + CuNCs, y-CDs + Cu^{2+} + GSH + CuNCs. (D) The FT-IR spectra of y-CDs in the absence and presence of Cu^{2+}.

Vis absorption peak appeared at 430 nm for y-CDs, which was attributed to the coordination between y-CDs and Cu^{2+}. The FT-IR spectrum of Fig. 3D exhibited that in the presence of Cu^{2+}, part of the infrared bands of y-CDs became broader, explaining the interaction between Cu^{2+} and y-CDs. The Raman spectrum (Fig. 4A) showed that the D and G bands of the y-CDs at 1373.3 and 1517.9 cm^{-1}, respectively, have significant changes in the presence of Cu^{2+}. The ratio of D band to G band changed from 0.87 to 1.37, which was also due to the coordination of y-CDs with Cu^{2+}. As depicted in the TEM image of Fig. 4B, the y-CDs were still in a dispersed state with the addition of Cu^{2+}. The above results were consistent with the results of the reported literature,[34] indicating that the coordination of y-CDs with Cu^{2+} inhibited the occurrence of PET, which increased the fluorescence of y-CDs. Therefore, in accordance with the recently reported mechanism,[42–44] the enhanced fluorescence of y-CDs might be due to the coordination of y-CDs containing amino groups with Cu^{2+} to inhibit the occurrence of PET.

To elucidate the possible mechanism for the quenched fluorescence of CuNCs caused by Cu^{2+}-(y-CDs) complexes, we have studied the UV-vis absorption, fluorescence lifetime decay spectra and zeta potentials. Fig. 4C described that the absorption spectrum of Cu^{2+}-(y-CDs) complexes partially overlapped with the excitation and emission spectra of CuNCs, suggesting that the fluorescence quenching was related to FRET or inner filter effect (IFE).[45,46] Then, the fluorescence lifetime of CuNCs before and after the addition of Cu^{2+}-(y-CDs) complexes were recorded to further investigate the possible quenching process. As represented in Fig. 4D, it was clear that the average lifetime of CuNCs decreased from 3.95 to 1.88 ns with the addition of Cu^{2+}-(y-CDs) complexes, which negated the IFE whose average lifetime hardly changed. Moreover, the zeta potentials of CuNCs were studied in the absence and presence of Cu^{2+}-(y-CDs) complexes. The zeta potential (Fig. 4E) of CuNCs changed from −15.66 to −10.33 mV after adding Cu^{2+}-(y-CDs) complexes, illustrating the existence of electrostatic

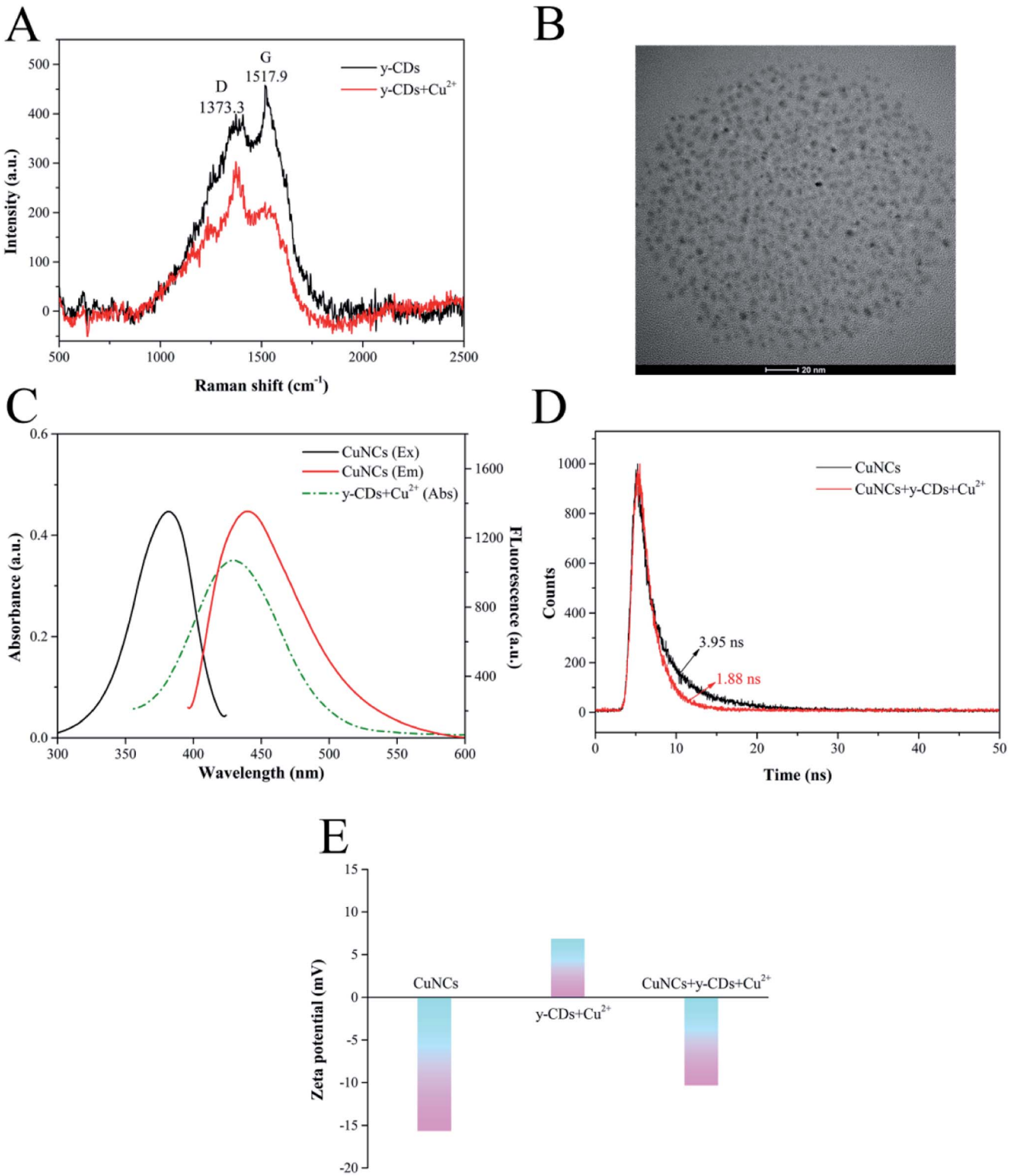

Fig. 4 (A) Raman scattering spectra of y-CDs in the absence and presence of Cu^{2+}. (B) TEM image of y-CDs in the presence of Cu^{2+}. (C) The fluorescence excitation (E_x) and emission (E_m) spectra of CuNCs and the UV-vis absorption (Abs) spectrum of y-CDs + Cu^{2+}. (D) The fluorescence lifetime decay spectra of CuNCs before and after the addition of y-CDs + Cu^{2+}. (E) The zeta potentials of CuNCs, y-CDs + Cu^{2+} and CuNCs + y-CDs + Cu^{2+}.

interaction between them. Hence, the above results suggested that the possible quenching mechanism was associated with FRET rather than IFE. For biothiols detection, in virtue of the strong affinity between biothiols and Cu^{2+}, the biothiols could inhibit the formation of Cu^{2+}-(y-CDs) complexes, resulting in a significant decrease in absorption at 430 nm (Fig. 3B) and

then weakening the FRET process between the Cu^{2+}-(y-CDs) complexes and the CuNCs. Thereby the fluorescence of y-CDs and CuNCs could be quenched and recovered, respectively.

3.4. Optimization of the experimental conditions

To establish an analytical performance for the determination of Cu^{2+} and biothiols, the reaction conditions including the concentration of y-CDs, pH, reaction temperature and time of the system were optimized. The best analytical performance was implemented by measuring the fluorescence intensity ratio (F_{567}/F_{450}) of y-CDs and CuNCs.

Initially, the optimal concentration of y-CDs affects the quantitative determination of the Cu^{2+}. The low concentration of y-CDs results in a narrow linear range of Cu^{2+}, while the high concentration is insensitive to Cu^{2+} detection. Thereby, the y-CDs concentration was optimized at first. As depicted in

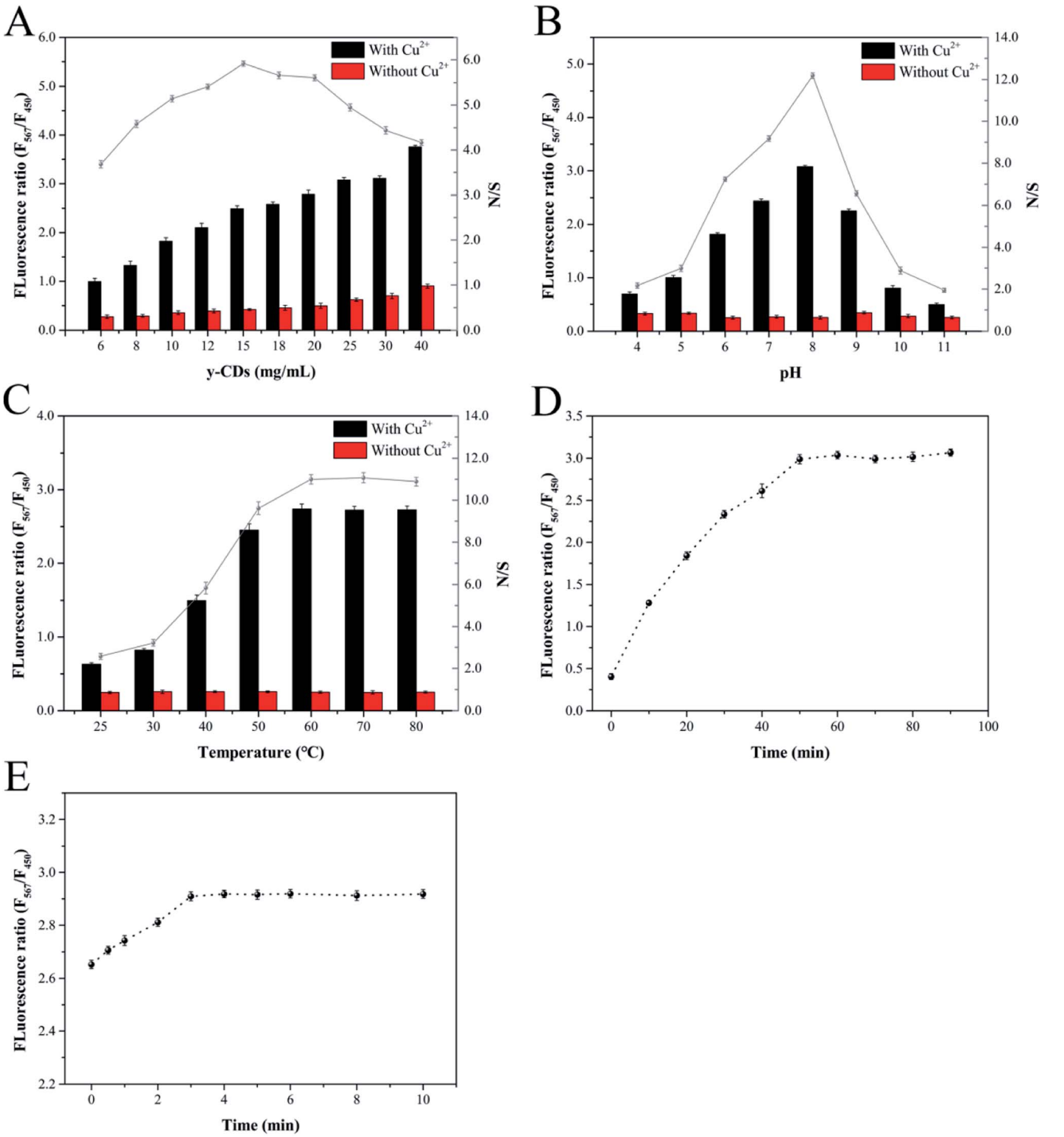

Fig. 5 The effects of various reactive conditions on the detection of Cu^{2+}: the concentration of y-CDs (A), the pH of reactive system (B), the temperature of reactive solution (C) and the reactive time of Cu^{2+} and CuNCs (D, E).

Fig. 5A, the relative ratio of the absence and presence of Cu^{2+} reached the maximum when the y-CDs concentration was 15 mg mL^{-1}. Thus, 15 mg mL^{-1} was selected as the optimum in this work. The pH of the method was investigated. Fig. 5B indicated that in the absence of Cu^{2+}, the intensity ratio hardly changed in the pH range of 4–11. However, with the introduction of Cu^{2+}, the fluorescent intensity ratio increased gradually in the range of 4–8 but rapidly decreased from 8 to 11. This phenomenon was associated with the protonation process of amino groups on y-CDs from pH 4–8 and the precipitation of $Cu(OH)_2$ and CuO in strong alkaline conditions, reducing the interaction between Cu^{2+} and y-CDs. Therefore, pH 8 was chosen as the optimized pH for further experiment.

As presented in Fig. 5C, in the absence of Cu^{2+}, the fluorescent intensity ratio almost unchanged with the temperature increasing. In the presence of Cu^{2+}, the fluorescence intensity ratio constantly increased and remained unchanged after 60 °C, which was consistent with the result of relative ratio. Hence, the reaction temperature of 60 °C was used in the following measurement. Fig. 5D displayed the influence of reaction time between Cu^{2+} and y-CDs. The results demonstrated that the fluorescence intensity ratio increased significantly, and reached equilibrium at 50 min. Fig. 5E showed that the fluorescence intensity ratio tended to stabilize after 3 min of reaction between CuNCs and Cu^{2+}-(y-CDs) complexes, and remained unchanged with the extension of time. So, 50 min and 3 min were considered to be the optimum reaction time in the two processes throughout the experiment, individually.

3.5. Ratiometric fluorescence determination for Cu^{2+} and biothiols

3.5.1. Detection of Cu^{2+}. Under the optimized conditions, the feasibility of ratiometric fluorescence probe based on y-CDs and CuNCs for Cu^{2+} detection was studied. As plotted in Fig. 6A, the fluorescence intensities of y-CDs at 567 nm gradually increased, whereas those of CuNCs at 450 nm was quenched slowly. Fig. 6B showed that the fluorescence intensity ratios increased constantly with the increase of Cu^{2+} concentrations in the range of 0–250 μM, and revealed good linear relationship

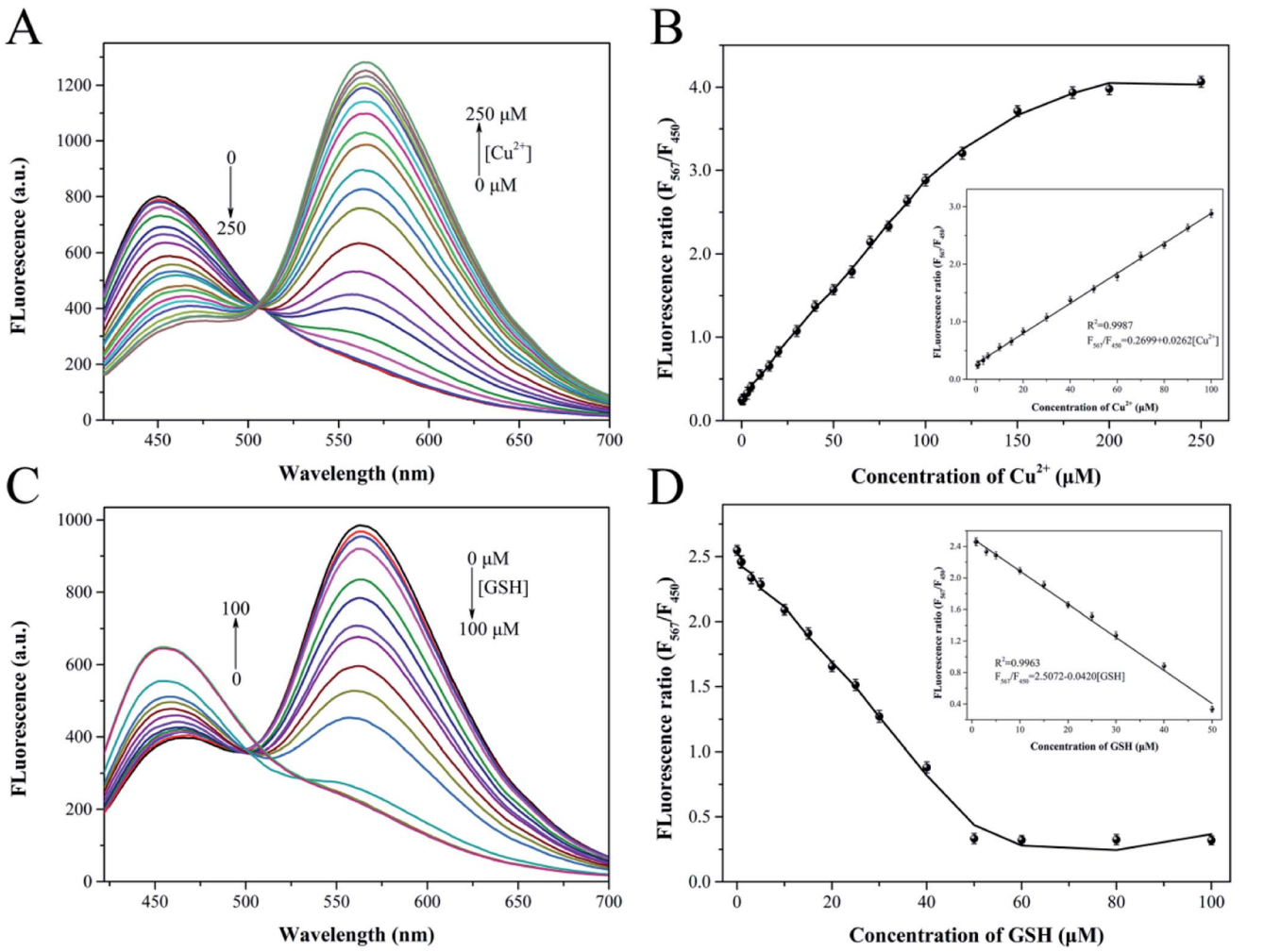

Fig. 6 Fluorescence responses of ratiometric fluorescence probe at different concentrations of (A) Cu^{2+} from 0 to 250 μM and (C) GSH from 0 to 100 μM. Plots of fluorescence intensity ratio of F_{567}/F_{450} *versus* the (B) Cu^{2+} and (D) GSH concentrations. Insets show the calibration curves of Cu^{2+} detection from 0.5 to 100 μM and GSH detection from 0.8 to 50 μM, respectively.

(F_{567}/F_{450} = 0.2699 + 0.0262 [Cu^{2+}], R^2 = 0.9987) with the Cu^{2+} concentrations in the range of 0.5–100 μM (inset in Fig. 6B). According to the rule of $3\sigma/k$, the limit of detection (LOD) was calculated as 0.21 μM that was much lower than the specified standard of Cu^{2+} in drinking water stipulated by US Environmental Protection Agency (EPA) of 20 μM and World Health Organization (WHO) of 30 μM.[47,48] Moreover, it was extremely clear that the linear range and LOD of Cu^{2+} detection in this study were comparable or even superior to the most of previously reported ratiometric fluorescence methods listed in Table S1.† Meanwhile, this ratiometric fluorescence probe was not only environmentally friendly, but also avoided the use of organic reagents and complicated synthesis processes.

3.5.2. Detection of biothiols. In order to balance the signal background and sensitivity, the concentration of Cu^{2+} was set to 70 μM during the detection of biothiols. Then, the performance of the ratiometric fluorescence probe composed of CuNCs and Cu^{2+}-(y-CDs) complexes was investigated through adding various concentrations of biothiols. Fig. 6C, S3A and C† represented that the fluorescence intensities of y-CDs at 567 nm gradually decreased, while those of CuNCs at 450 nm restored slowly. The fluorescence intensity ratios gradually decreased when the concentrations of biothiols varied from 0 to 100 μM, and varied linearly with biothiols in the concentration ranges of 0.8–50 μM (inset in Fig. 6D, S3B and D†). The linear regression equations were expressed as F_{567}/F_{450} = 2.5072–0.0420 [GSH] (R^2 = 0.9963), F_{567}/F_{450} = 2.2820–0.0358 [Cys] (R^2 = 0.9966) and F_{567}/F_{450} = 2.3605–0.0309 [Hcy] (R^2 = 0.9972), respectively. And the LODs based on $3\sigma/k$ rule were calculated as 0.33 μM, 0.39 μM and 0.46 μM for GSH, Cys and Hcy, respectively. Table S2† summarized several recently reported ratiometric fluorescence methods for the detection of biothiols. Compared with other methods, this ratiometric fluorescence probe had higher sensitivity and wider response range, exhibiting excellent performance for biothiols detection.

3.6. Selectivity for Cu^{2+} and biothiols detection

The selectivity of the proposed ratiometric fluorescent probe for the determination of Cu^{2+} and biothiols was evaluated by investigating the influences of some potential interfering substances. The fluorescence responses of the probe toward Cu^{2+} and other metal ions including Ag^+, Al^{3+}, Ba^{2+}, Ca^{2+}, Cd^{2+}, Fe^{3+}, Hg^{2+}, K^+, Li^+, Mg^{2+}, Mn^{2+}, Na^+, Ni^{2+}, Pb^{2+} and Zn^{2+} were illustrated in Fig. 7A. The results indicated that the fluorescent intensity ratio increased significantly after adding Cu^{2+}, whereas the other metal ions caused inappreciable changes. The specific recognition of this ratiometric fluorescence system toward Cu^{2+} could be attributed to the thermodynamic affinity and chelation between "N" of y-CDs and Cu^{2+}.[41] Besides, the fluorescence responses of the probe to Cu^{2+} were not affected by the coexisting Cu^{2+} and other metal ions. Therefore, the proposed ratiometric fluorescence probe displayed highly selectivity toward Cu^{2+}. We subsequently verified the fluorescence responses of the ratiometric fluorescence probe to the other 19 amino acids (Ala, Arg, Asn, Asp, Gln, Glu, Gly, His, Leu, Lys, Met, Phe, Pro, Ser, The, Thr, Trp, Tyr, Val) to assess the specific binding interaction of biothiols toward Cu^{2+}. As shown in Fig. 7B, the fluorescence intensity ratios represented negligible variations in the presence of these amino acids, while the fluorescent intensity ratios decreased obviously in the presence of biothiols, indicating that only biothiols could quench the fluorescence of y-CDs and restore that of CuNCs. This situation was related to the –SH groups contained in the biothiols, which could chelate with Cu^{2+} to form the Cu–S bonds.[49] As a consequence, the above results suggested that this method had excellent selectivity toward biothiols detection.

3.7. Detection of Cu^{2+} and biothiols in real samples

To investigate the feasibility and applicability of the proposed ratiometric fluorescent probe, we performed the measurements of Cu^{2+} in tap water, river water, grape juice, peach juice samples and biothiols in human serum samples, respectively. Three concentrations of Cu^{2+} (5.0 μM, 50.0 μM and 80.0 μM) were respectively added to the water and beverage samples to prepare spiked samples and then the fluorescence intensity ratios were measured as aforesaid conditions. As summarized in Table 1, the recoveries for Cu^{2+} detection ranged from 97.7% to 103.7% in tap water sample, 95.3% to 102.0% in river water sample, 99.5% to 101.4% in grape juice sample and 100.3% to 101.3% in peach juice sample with desirable relative standard

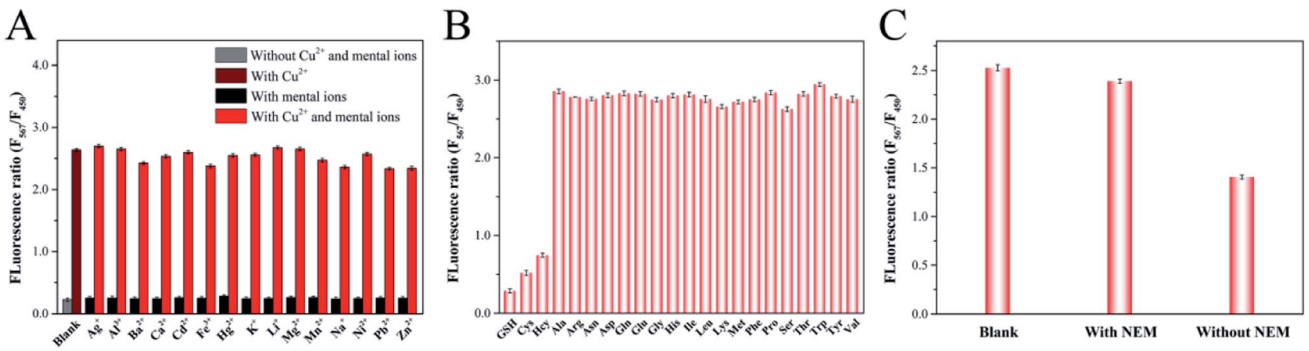

Fig. 7 (A) Responses of ratiometric fluorescence probe in the presence of various metal ions (500 μM) and their mixture with Cu^{2+} (100 μM). (B) Ratiometric fluorescence responses to 19 essential amino acids (100 μM) and biothiols (50 μM). (C) Responses of ratiometric fluorescence probe to serum with or without pretreatment by *N*-ethylmaleimide (NEM).

Table 1 Determination of Cu^{2+} in real samples by this method (n=3)[a]

Samples	Added (μM)	Found (μM)	Recovery (%)	RSD (%)
Tap water	0	ND	—	—
	5.0	5.2	103.7	1.7
	50.0	48.9	97.7	1.4
	80.0	80.2	100.2	2.5
River water	0	ND	—	—
	5.0	5.2	102.0	1.0
	50.0	50.6	100.7	1.9
	80.0	76.5	95.3	2.0
Grape juice	0	ND	—	—
	5.0	5.1	101.4	1.9
	50.0	50.6	100.9	1.1
	80.0	79.7	99.5	1.3
Peach juice	0	ND	—	—
	5.0	5.1	100.3	1.7
	50.0	51.0	101.3	3.0
	80.0	80.7	100.5	1.2

[a] ND: not detected.

Table 2 Determination of biothiols in human serum samples by this method (n=3)

Sample	Added GSH (μM)	Found (μM)	Recovery (%)	RSD (%)
Serum	0	14.97	—	—
	5.0	19.8	96.2	1.4
	15.0	30.4	102.9	1.7
	30.0	43.9	96.5	3.2

deviations (RSDs), respectively. In the following biothiols assays, it was found in Fig. 7C that the addition of serum sample into the probe led to an obvious reduction in fluorescence intensity ratio. In contrast, the fluorescence intensity ratio of serum sample pretreated with *N*-ethylmaleimide (NEM), a thiol blocking reagent, presented no significant change, suggesting that the decrease in fluorescence intensity ratio was ascribed to the biothiols in the serum sample.[50] Then, we selected GSH as the standard to analyze the contents of biothiols in serum sample. As shown in Table 2, after spiking the serum samples with certain concentrations of GSH (5.0 μM, 15.0 μM and 30.0 μM), the recoveries of GSH in the serum samples ranged from 96.2% to 102.9% with RSD of around 1.4% to 3.2%. All of these results demonstrated that the proposed ratiometric fluorescent probe provided great potential for Cu^{2+} and biothiols assays in real samples.

4. Conclusion

In summary, we have successfully established a simple and effective dual-emission ratiometric fluorescent probe based on y-CDs and CuNCs, and demonstrated the potential of this probe for highly sensitive determination of Cu^{2+} and biothiols. This type of probe, which displayed the advantages of simple synthesis, environmental friendliness and multi targets detection, was established by self-assembling between y-CDs and CuNCs. In the presence of Cu^{2+}, y-CDs could chelate with Cu^{2+} to form Cu^{2+}-(y-CDs) complexes that could enhance the fluorescence of y-CDs owing to the inhibition of the PET and quench the fluorescence of CuNCs due to FRET between CuNCs and Cu^{2+}-(y-CDs) complexes. After introducing biothiols, the fluorescence of y-CDs was quenched, whereas that of CuNCs was restored, which was attributed to that the stronger interaction between biothiols and Cu^{2+} released Cu^{2+} from the y-CDs surface. Thus, the ratiometric fluorescence method provided a novel strategy for Cu^{2+} determination in water and beverage samples, and biothiols in human serum samples, showing its potential application in real samples detection.

Author contributions

Ning Zhao: conceptualization, methodology, formal analysis, investigation, writing – original draft. Jianqiang Song: writing – review & editing. Zheng Huang: writing – review & editing. Longshan Zhao: writing – review & editing, supervision, project administration.

Conflicts of interest

There are no conflicts to declare.

Acknowledgements

This work was supported by Hainan Provincial Philosophy and Social Science Planning Project (HNSK(YB)20-64), the Middle-aged Backbone Personnel Training Program of Shenyang Pharmaceutical University (ZQN2016011), Scientific Research Fund of Liaoning Provincial Education Department (2020LZD02), Inter-school Cooperation Project of General Undergraduate Universities in Liaoning Province (2020-181), Project of Shenyang Key Laboratory of Functional Drug Carrier Materials (Grant No. 19-110-4-08).

References

1 F. C. Coelho, R. Squitti, M. Ventriglia, G. Cerchiaro, J. P. Daher, J. G. Rocha, M. C. A. Rongioletti and A. C. Moonen, *Biomolecules*, 2020, **10**, 897.
2 J. Chen, Y. Jiang, H. Shi, Y. Peng, X. Fan and C. Li, *Pflügers Archiv*, 2020, **472**, 1415–1429.
3 S. W. Cho, A. S. Rao, S. Bhunia, Y. J. Reo, S. Singha and K. H. Ahn, *Sens. Actuators, B*, 2019, **279**, 204–212.
4 J. Dai, C. Ma, P. Zhang, Y. Fu and B. Shen, *Dyes Pigm.*, 2020, **177**, 108321.
5 P. P. Praveen Kumar, N. Kaur, A. Shanavas and P. P. Neelakandan, *Analyst*, 2020, **145**, 851–857.
6 J. Wang, Y. Liu, M. Jiang, Y. Li, L. Xia and P. Wu, *Chem. Commun.*, 2018, **54**, 1004–1007.
7 C. K. de Andrade, P. M. K. de Brito, V. E. Dos Anjos and S. P. Quinaia, *Food Chem.*, 2018, **240**, 268–274.
8 X. Wei, H. Hu, B. Zheng, Z. Arslan, H. C. Huang, W. Mao and Y. M. Liu, *Anal. Methods*, 2017, **9**, 724–728.

9 M. El Badry Mohamed, E. Y. Frag and M. H. El Brawy, *Microchem. J.*, 2021, **164**, 106065.
10 P. Kamnoet, W. Aeungmaitrepirom, R. F. Menger and C. S. Henry, *Analyst*, 2021, **146**, 2229–2239.
11 L. Feng, L. Wu, F. Xing, L. Hu, J. Ren and X. Qu, *Biosens. Bioelectron.*, 2017, **98**, 378–385.
12 G. Wu, J. Zhou, X. Jiang, X. Guo and F. Gao, *Electrocatal*, 2013, **4**, 17–23.
13 J. Lin, P. Ni, Y. Sun, Y. Wang, L. Wang and Z. Li, *Sens. Actuators, B*, 2018, **255**, 3472–3478.
14 M. Ozyurek, S. Baki, N. Gungor, S. E. Celik, K. Guclu and R. Apak, *Anal. Chim. Acta*, 2012, **750**, 173–181.
15 M. J. Molaei, *RSC Adv.*, 2019, **9**, 6460–6481.
16 Y. Wang, J. Xu, L. Lei, F. Wang, Z. Xu and W. Zhang, *Sens. Actuators, B*, 2018, **264**, 296–303.
17 C.-L. Shen, Q. Lou, K.-K. Liu, L. Dong and C.-X. Shan, *Nano Today*, 2020, **35**, 100954.
18 H. Ehtesabi, M. Amirfazli, F. Massah and Z. Bagheri, *Adv. Nat. Sci.: Nanosci. Nanotechnol.*, 2020, **11**, 025017.
19 Y. Ma, Y. Cen, M. Sohail, G. Xu, F. Wei, M. Shi, X. Xu, Y. Song, Y. Ma and Q. Hu, *ACS Appl. Mater. Interfaces*, 2017, **9**, 33011–33019.
20 Z. Qian, X. Shan, L. Chai, J. Ma, J. Chen and H. Feng, *ACS Appl. Mater. Interfaces*, 2014, **6**, 6797–6805.
21 S. J. Zhu, Y. B. Song, X. H. Zhao, J. R. Shao, J. H. Zhang and B. Yang, *Nano Res.*, 2015, **8**, 355–381.
22 Y. Su, T. Xue, Y. Liu, J. Qi, R. Jin and Z. Lin, *Nano Res.*, 2019, **12**, 1251–1265.
23 H. T. Sun and Y. Sakka, *Sci. Technol. Adv. Mater.*, 2014, **15**, 14205.
24 H. Rao, H. Ge, Z. Lu, W. Liu, Z. Chen, Z. Zhang, X. Wang, P. Zou, Y. Wang, H. He and X. Zeng, *Microchim. Acta*, 2016, **183**, 1651–1657.
25 L. Zhang, Z. Wang, J. Hou, L. Lei, J. Li, J. Bai, H. Huang and Y. Li, *Anal. Methods*, 2018, **10**, 2560–2566.
26 H. E. Okda, S. El Sayed, I. Otri, R. C. M. Ferreira, S. P. G. Costa, M. M. M. Raposo, R. Martínez-Máñez and F. Sancenón, *Dyes Pigm.*, 2019, **162**, 303–308.
27 Q. Dai, W. Liu, X. Zhuang, J. Wu, H. Zhang and P. Wang, *Anal. Chem.*, 2011, **83**, 6559–6564.
28 M. Lan, J. Zhang, Y. S. Chui, P. Wang, X. Chen, C. S. Lee, H. L. Kwong and W. Zhang, *ACS Appl. Mater. Interfaces*, 2014, **6**, 21270–21278.
29 M. H. Lee, J. S. Kim and J. L. Sessler, *Chem. Soc. Rev.*, 2015, **44**, 4185–4191.
30 H. H. Zeng, Z. Y. Zhou, F. Liu, J. Deng, S. Y. Huang, G. P. Li, P. Q. Lai, Y. P. Xie and W. Xiao, *Analyst*, 2019, **144**, 7368–7377.
31 R. Ying, H. Lu and S. Xu, *New J. Chem.*, 2019, **43**, 6404–6410.
32 T. Luo, S. Zhang, Y. Wang, M. Wang, M. Liao and X. Kou, *Luminescence*, 2017, **32**, 1092–1099.
33 J. Lu, J. X. Yang, J. Wang, A. Lim, S. Wang and K. P. Loh, *ACS Nano*, 2009, **3**, 2367–2375.
34 W. Lv, M. Lin, R. Li, Q. Zhang, H. Liu, J. Wang and C. Huang, *Chin. Chem. Lett.*, 2019, **30**, 1410–1414.
35 M. Vedamalai, A. P. Periasamy, C. W. Wang, Y. T. Tseng, L. C. Ho, C. C. Shih and H. T. Chang, *Nanoscale*, 2014, **6**, 13119–13125.
36 J. Song, N. Zhao, Y. Qu and L. Zhao, *Dyes Pigm.*, 2021, **193**, 109564.
37 L. Wang, H. Miao, D. Zhong and X. Yang, *Anal. Methods*, 2016, **8**, 40–44.
38 Y. Jiao, Y. Gao, Y. Meng, W. Lu, Y. Liu, H. Han, S. Shuang, L. Li and C. Dong, *ACS Appl. Mater. Interfaces*, 2019, **11**, 16822–16829.
39 N. Zhao, Y. Wang, S. Hou and L. Zhao, *Microchim. Acta*, 2020, **187**, 351.
40 S. Momeni, R. Ahmadi, A. Safavi and I. Nabipour, *Talanta*, 2017, **175**, 514–521.
41 S. Liu, J. Tian, L. Wang, Y. Zhang, X. Qin, Y. Luo, A. M. Asiri, A. O. Al-Youbi and X. Sun, *Adv. Mater.*, 2012, **24**, 2037–2041.
42 A. Saravanan, G. Subashini, S. Shyamsivappan, T. Suresh, K. Kadirvelu, N. Bhuvanesh, R. Nandhakumar and P. S. Mohan, *J. Photochem. Photobiol., A*, 2018, **364**, 424–432.
43 X. Wang, Z. Yu, J. Wang, J. Shen, Y. Lu, W. Shen, Y. Lv and X. Sun, *J. Photochem. Photobiol., A*, 2018, **357**, 49–59.
44 Z. Shi, Y. Tu, R. Wang, G. Liu and S. Pu, *Dyes Pigm.*, 2018, **149**, 764–773.
45 D. Song, R. Yang, S. Fang, Y. Liu and F. Long, *Microchim. Acta*, 2018, **185**, 508.
46 S. Chen, Y. L. Yu and J. H. Wang, *Anal. Chim. Acta*, 2018, **999**, 13–26.
47 J. Liu and Y. Lu, *J. Am. Chem. Soc.*, 2007, **129**, 9838–9839.
48 WHO, *WHO Guidelines Values for Chemicals That Are of Health Significance in Drinking Water, Guidelines for Drinking Water Quality*, WHO, Geneva, 3rd edn, 2008.
49 Z.-Q. Hu, L.-L. Sun, Y.-Y. Gu and Y. Jiang, *Sens. Actuators, B*, 2015, **212**, 220–224.
50 L. Zhou, Y. Lin, Z. Huang, J. Ren and X. Qu, *Chem. Commun.*, 2012, **48**, 1147–1149.